Rates and Stoichiometries of Metal Ion Probes of Cysteine Residues within Ion Channels

Lai-Sheung Choi, Tivadar Mach, and Hagan Bayley*
Department of Chemistry, University of Oxford, Oxford, United Kingdom

ABSTRACT Metal ion probes are used to assess the accessibility of cysteine side chains in polypeptides lining the conductive pathways of ion channels and thereby determine the conformations of channel states. Despite the widespread use of this approach, the chemistry of metal ion-thiol interactions has not been fully elucidated. Here, we investigate the modification of cysteine residues within a protein pore by the commonly used Ag^+ and Cd^{2+} probes at the single-molecule level, and provide rates and stoichiometries that will be useful for the design and interpretation of accessibility experiments.

INTRODUCTION

Ion channels play key roles in the electrical excitability of cells and in synaptic transmission, enabling physiological activities as diverse as memory storage and muscle contraction. Crucially, ion channels regulate the selective passive flow of permeant ions through membranes by transitions between closed and open conformational states. The dynamics of these transitions can be studied in detail with the use of electrophysiological techniques. However, additional information is required to understand the molecular bases of the underlying protein conformational changes, and in this regard the substituted-cysteine accessibility method (SCAM) (1) combined with x-ray crystallography (2) has been highly informative.

Two types of thiol-specific reagents are commonly used as probes in SCAM, namely, thiophilic metal ions (e.g., Ag^+ (3), Cd^{2+} (4), Zn^{2+} (5), and Hg^{2+} (6)) and electrophilic reagents (e.g., methanethiosulfonates (7)). The thiophilic metal ions have sizes (8) and water exchange rates (9) similar to those of natural permeant ions, and therefore are expected to pass through the channel or be prevented from doing so in accord with the channel state (open, closed, desensitized, etc.). Hence, the accessibility of cysteine residues introduced by, e.g., scanning mutagenesis, reveals information about the structures of conformational states. The ability of these metal ions to form multiply coordinated complexes has also been used to reveal the spatial proximity of amino acid residues located on different subunits of ion channels (10).

Here, we use the staphylococcal α-hemolysin (αHL) transmembrane pore (11) as a nanoreactor (12) to examine metal ion-thiol chemistry at the single-molecule level. Reaction sites can be engineered into the lumen of the αHL pore and have been used to examine a variety of chemical interactions (12), including the interactions of divalent metal ions with histidine side chains (13) and EDTA-like chelators (14). In this work, we used a cysteine-containing αHL pore (P_C) to study the kinetics and stoichiometry of two commonly used metal ion probes (Ag^+ and Cd^{2+}) with a thiol group. We also examined the effects of neighboring cysteine and histidine side chains.

MATERIALS AND METHODS

Mutagenesis at multiple widely separated sites

The αHL AG gene encodes a polypeptide with four mutations (Lys-8→Ala, Met-113→Gly, Lys-131→Gly, and Lys-147→Gly) and was constructed from the template pT7-WT-αHL (15). Another gene, G137C-AG, encodes an αHL polypeptide containing the same four mutations, with an additional Gly-137→Cys mutation and an extension of eight-aspartate residues at the C-terminus, and was constructed from the template pT7-G137C-D8-RL3 (16). RL3 is a version of the WT αHL gene with silent mutations in the segment of the gene that encodes the region around and within the stem domain. These mutations produce six new restriction sites (17). Both αHL AG and αHL G137C-AG (C) were constructed by means of multiple site-directed mutagenesis (QuikChange Lightning Multi Site-Directed Mutagenesis Kit, catalog no. 210515; Agilent Technologies, Berkshire, UK). For the AG gene, a polymerase chain reaction (PCR) was carried out with the following four sense primers: K8A, 5′-GCAG ATTCTGATATTAATATTGCAACCGGTACTACAGATATTGGAAGC-3′; WT_M113G, 5′-CGATTGATACAAAAGAGTATGGGAGTACTTTAACT TATGGATTCAACGG-3′; WT_K131G, 5′-TTACTGGTGATGATACAG GAGGAATTGGCGGCCTTATTGGTG-3′; WT_K147G, 5′-GTTTCG ATTGGTCATACACTGGGATATGTTCAACCTGATTTCAAAAC-3′. For G137C-AG, a PCR was carried out with the following four sense primers: K8A, 5′-GCAGATTCTGATATTAATATTGCAACCGGTACTACAGATAT TGGAAGC-3′; RL3_M113G, 5′-GAATTCGATTGATACAAAAGAG TATGGGAGTACGTTAACGTACGGATTC-3′; G137C_RL3_K131G, 5′-GTTACTGGTGATGATACAGGAGGAATTGGAGGCCTTATTTGCGC-3′; RL3_K147G, 5′-GTTTCGATTGGTCATACACTTGGGTATGTTCAA CCTGATTTCAAAAC-3′. The codons for the mutated amino acid residues are underlined. The *AflII* restriction site in pT7-G137C-D8-RL3 was removed by the K147G mutation.

The procedure was similar to that suggested in the kit, with slight modifications. Each PCR (25 μL) was set up by mixing the following reagents in the order listed: 10× QuikChange Lightning Multi reaction buffer

Submitted December 11, 2012, and accepted for publication April 25, 2013.

*Correspondence: hagan.bayley@chem.ox.ac.uk

Editor: William Kobertz.

0006-3495/13/07/0356/9 $2.00

http://dx.doi.org/10.1016/j.bpj.2013.04.046

(2.5 μL), nuclease-free water (to make up the final volume of the reaction to 25 μL), double-stranded plasmid DNA template (50–100 ng), mutagenic primers (~100 ng of each primer), deoxynucleotide (dNTP) mix (1 μL from the kit), and the QuikChange Lightning Multi enzyme blend (1 μL). The PCRs were carried out with following program: 94°C for 5 min, 18 cycles of 95°C (0.5 min), 55°C (0.5 min), 68°C (9 min), followed by a final extension at 68°C for 7 min. The PCRs were then cooled and the template was digested with *DpnI* (1 μL, supplied with the kit) at 37°C for 1.5 h. pT7 plasmids containing the mutant genes were generated by transforming *Escherichia coli* XL-10 Gold ultracompetent cells with the PCR product. The DNA sequences of the genes were verified (Source BioScience).

Further site-directed mutagenesis

The genes αHL L135H/G137C-AG (HC), αHL L135C/G137C-AG (CC), and αHL L135H-AG (H) were constructed by using pT7-G137C-AG (see above) as the template. For the HC gene, two PCRs (Phusion Flash PCR Master Mix, catalog No. F-548S; Finnzymes/Thermo Scientific, Leicestershire, UK) were carried out with the following two sets of primers: first set: mutagenic primer (sense, L135H-G137C-fw) 5′-CAGGAGGAATTG GAGGCCATATTTGCGCAAATGTTTC-3′, nonmutagenic primer (antisense, SC47) 5′-CAGAAGTGGTCCTGCAACTTTAT-3′; second set: mutagenic primer (antisense, L135H-G137C-rev) 5′-GAAACATTTGCG CAAATATGGCCTCCAATTCCTCCTG-3′, nonmutagenic primer (sense, SC46) 5′-ATAAAGTTGCAGGACCACTTCTG-3′. For the CC gene, two PCRs were carried out with the following two sets of primers: first set: mutagenic primer (sense, L135C-G137C-fw) 5′-GATACAGGAGGAAT TGGAGGCTGTATTTGCGCAAATGTTTCGAT-3′, nonmutagenic primer (antisense, SC47) 5′-CAGAAGTGGTCCTGCAACTTTAT-3′; second set: mutagenic primer (antisense, L135C-G137C-rev) 5′-ATCGAAACAT TTGCGCAAATACAGCCTCCAATTCCTCCTGTATC-3′, nonmutagenic primer (sense, SC46) 5′-ATAAAGTTGCAGGACCACTTCTG-3′. For the H gene, two PCRs were carried out with the following two sets of primers: first set: mutagenic primer (sense, L135H-C137G-fw) 5′-GATACAGGA GGAATTGGAGGCCATATTGGTGCAAATGTTTCGATTGGTC-3′, nonmutagenic primer (antisense, SC47) 5′-CAGAAGTGGTCCTGCAACTT TAT-3′; second set: mutagenic primer (antisense, L135H-C137G-rev) 5′-GACCAATCGAAACATTTGCACCAATATGGCCTCCAATTCCTCCTG TATC-3′, nonmutagenic primer (sense, SC46) 5′-ATAAAGTTGCAGGAC CACTTCTG-3′. Notice that in the H gene, Cys-137 is mutated back into the αHL WT residue glycine. The mutated codons are underlined.

The template DNA, pT7-G137C-AG (100 ng μL^{-1}), was linearized with *NdeI* for the first primer set and with *HindIII* for the second set. Each PCR (20 μL) was set up by mixing the following reagents: Phusion Flash PCR Master Mix (10 μL, 2×), the digested template DNA (1 μL, 10 ng μL^{-1}), the two primers (1 μL each, 10 μM), and nuclease-free water (7 μL). The PCR reactions were carried out with following program: 98°C for 30 s, 30 cycles of 98°C (10 s), 68°C (5 s), 72°C (40 s), followed by a final extension at 72°C for 60 s. The two PCR products (5 μL each) for a particular mutation were mixed and used to transform *E. coli* XL-10 Gold cells, which generated the pT7 vector containing the mutant gene by in vivo recombination. The DNA sequences of the genes were verified (Source BioScience).

Protein preparation

The heteroheptameric cysteine-containing αHL pores (P_C, P_{HC}, P_{CC}, and P_H) were prepared as described by Choi and Bayley (18). P_C, P_{HC}, P_{CC}, and P_H represent $(AG)_6(G137C\text{-}AG)_1$, $(AG)_6(L135H/G137C\text{-}AG)_1$, $(AG)_6(L135C/G137C\text{-}AG)_1$, and $(AG)_6(L135H\text{-}AG)_1$ respectively. In brief, pT7 plasmids carrying mutated αHL genes were produced by site-directed mutagenesis (see above). αHL proteins were expressed in the presence of [^{35}S]methionine in an *E. coli* in vitro transcription and translation (IVTT) system (*E. coli* T7 S30 Extract System for Circular DNA, catalog No. L1130; Promega, Southampton, UK). Protein expression and oligomerization were carried out simultaneously by resuspending rabbit red blood cell membranes (rRBCm) in the IVTT mixture before incubation at 37°C for 1.5 h. To prepare heteroheptamers (e.g., P_C), the plasmid DNAs for AG and G137C-AG were mixed in a 6:1 ratio for IVTT (50 μL). αHL heteroheptamers were purified in a 5% SDS-polyacrylamide gel with 1× Tris-Glycine-SDS (TGS) running buffer under reducing conditions. The gel was dried and the protein bands were visualized by autoradiography. Because the G137C-AG monomer has an extension of eight aspartate residues at the C-terminus (similarly to the L135H/G137C-AG, L135C/G137C-AG, and L135H-AG monomers), but the AG monomer does not, heteroheptamers containing G137C-AG subunits carry more negative charge and migrate more rapidly toward the anode (19). Therefore, the target heteroheptamer, P_C, with a 6:1 ratio of AG to G137C-AG corresponds to the band immediately beneath the $(AG)_7$ band on a gel (Fig. 1). The P_C band was cut out and rehydrated, and the protein was extracted (18). Purified proteins were stored at –80°C in TE buffer (10 mM Tris.HCl, 1 mM EDTA, pH 8.0) containing 5 mM dithiothreitol (DTT).

Planar lipid bilayer recordings

Lipid bilayers were formed from 1,2-diphytanoyl-*sn*-glycero-3-phosphocholine (DPhPC; Avanti Polar Lipids, Alabaster, AL) in a previously described apparatus (20). Buffer solutions (2 M KNO_3, 10 mM MOPS, with 10 mM EDTA or treated with Chelex ion-exchange resin, adjusted to pH 7.4 with 1 M KOH) were deoxygenated by purging with N_2 for 15–20 min before use. Buffer (1 mL) was added to both compartments of the apparatus and a potential was applied across the bilayer with Ag/AgCl electrodes that were in double-layered agarose bridges. The electrodes were covered with an inner layer of 3 M KCl in 3% low-melting agarose, which was encased in an outer layer of 2 M KNO_3 in 3% low-melting agarose. The bridges were necessary because silver ions leach from bare Ag/AgCl electrodes into high-chloride buffer solutions and react with thiol groups of the αHL pore. P_C (or P_{HC}, P_{CC}, or P_H) was added to the *cis* compartment (ground) and the applied potential was increased to +140 mV. The *cis* solution was stirred until a single channel appeared. Due to the denaturing effect of high concentrations of KNO_3 (≥1 M) on nonmembrane-associated αHL, αHL was inserted under asymmetrical salt conditions (150 mM KNO_3 (*cis*)/2 M KNO_3 (*trans*), both with same concentration of buffering agent and EDTA). After insertion, portions of the buffer in the *cis* compartment were replaced with 2.5 M KNO_3 buffer until the concentration of KNO_3 on the *cis* side reached 2 M. Current recordings were performed at 22°C ± 1°C with a patch-clamp amplifier (Axopatch 200B; Axon Instruments, now Molecular Devices, Berkshire, UK). The signal was filtered with a low-pass Bessel filter (80 dB/decade) with a corner frequency of 2 kHz, and sampled at 20 kHz with a DigiData 1320 A/D converter (Axon Instruments).

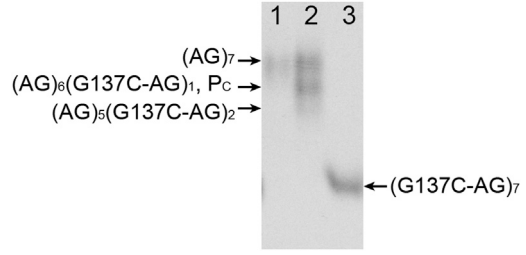

FIGURE 1 SDS-PAGE gel (5%) showing the bands corresponding to αHL heptamers. Lane 1: Heptamer made from AG monomer only. Lane 2: Heptamers formed from AG monomer and G137C-AG monomer mixed in a 6:1 ratio. Lane 3: Heptamer comprising G137C-AG monomer only. The identity of each band is indicated.

Freshly thawed aliquots of protein were used each day. Stock $AgNO_3$ (1 mM) and $Cd(NO_3)_2$ (10 mM) solutions in deionized water were prepared daily. The $AgNO_3$ solution was kept in the dark.

Data analysis of single-channel recordings

Current traces were filtered digitally with a 200 Hz low-pass Bessel filter (eight-pole) in Clampfit 9.2 (Axon Instruments). Events were detected by using the single-channel search feature. The mean dwell times ($\bar{\tau}$) of the current states were determined by fitting dwell-time histograms to single-exponential functions. Further analysis was carried out by using the program QuB (www.qub.buffalo.edu) to determine the rates (s^{-1}) for each transition. The processed data were plotted by using OriginPro 8.1 SR3 (OriginLab Corporation, Northampton, MA).

Owing to the low solubility of Ag^+ in chloride-containing solutions and the formation of complexes between Ag^+ and Cl^-, buffer solution containing KNO_3 as the electrolyte was used for Ag^+ binding studies. Moreover, 10 mM EDTA was present as a buffering agent for Ag^+ ion. $[Ag^+]_{free}$ was calculated with the program Maxchelator (http://maxchelator.stanford.edu) by using the stability constants appropriate under our conditions. The $\log_{10}$ value of the association constant for Ag^+ ion and the fully deprotonated form of EDTA is 7.32 ± 0.05 (22). The six pK_a values of EDTA are incorporated into the program (4, 8, 16, and 32 μM of added $AgNO_3$ correspond to 16, 33, 66, and 133 nM $[Ag^+]_{free}$). Similar values for $[Ag^+]_{free}$ were obtained with the program ALEX (23). Cd^{2+} binding was carried out in EDTA-free buffer; $[Cd^{2+}]_{free}$ is assumed to be the same as the total concentration of $Cd(NO_3)_2$ added.

RESULTS AND DISCUSSION

Design of the αHL mutant for metal ion detection

The homoheptameric wild-type αHL pore $(WT)_7$, which contains no cysteine residues, interacted with the metal ions under examination. In particular, Ag^+ bound reversibly to $(WT)_7$. This is presumably due to the affinity of Ag^+ for amino acid side chains in the pore lumen that contain nitrogen or sulfur atoms (24–27), such as those of lysine, arginine, histidine, and methionine. Therefore, potentially interacting residues located in the narrower regions of the lumen (the *cis* entrance and the β barrel) were mutated to noninteracting residues such as glycine and alanine. Other potentially interacting residues located in the wider vestibule region of the lumen and on the exterior of the pore were not mutated, because metal ion binding to these residues was not expected to cause detectable events. On this basis, the mutant αHL AG, which contains four point mutations (K8A/M113G/K131G/K147G), was designed (Fig. 2). Gratifyingly, $(AG)_7$ did not interact with Ag^+ and Cd^{2+}, and therefore it was used to provide the noise-free background for this study.

Based on this finding, a heteroheptameric αHL pore P_C with one cysteine-containing subunit (αHL G137C-AG) and six cysteine-free subunits (αHL AG; Fig. 2) was prepared. The side chain of the single cysteine residue points into the water-filled lumen of the pore.

Ag^+ binding

Ag^+ ($[Ag^+]_{free}$, 16–133 nM) added to the *cis* side of a bilayer containing a single P_C pore at –50 mV and pH 7.4 (2 M KNO_3, 10 mM MOPS, 10 mM EDTA) generates reversible blockades that show two current levels relative to the unoccupied pore ($\Delta I = 1.6 \pm 0.3$ pA (level 1) and $\Delta I = 3.6 \pm 0.6$ pA (level 2); $n = 3$; Fig. 3 *A*). The frequency of occurrence of these blockades increases with $[Ag^+]_{free}$, and at higher $[Ag^+]_{free}$, level 2 becomes more prominent than level 1. Transitions between unoccupied P_C (level 0) and level 2 always pass through level 1; direct transitions are not observed.

The rate constants for the transitions (Table 1) were determined from plots of the measured rates versus $[Ag^+]_{free}$ (Fig. 3 *C*, see also the Materials and Methods section), with the assumption that $[Ag^+]_{free}$ inside the pore is the same as that in bulk solution. Both the transition rate (v) from level 0 to level 1 (0→1) and that from level 1 to level 2 (1→2) have a first-order dependence on $[Ag^+]_{free}$: $v_{01} = k_{Ag,01}[Ag^+]_{free}$ and $v_{12} = k_{Ag,12}[Ag^+]_{free}$, where

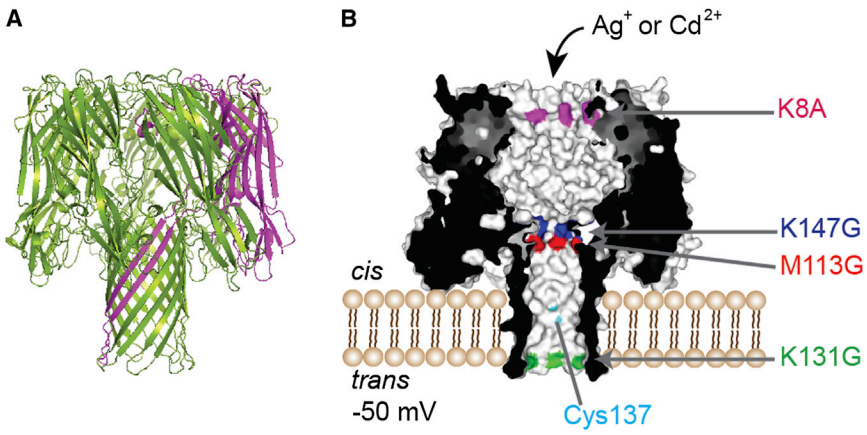

FIGURE 2 Structures of the αHL pores used for the metal-binding studies. (*A*) WT αHL is a mushroom-shaped transmembrane protein pore made of seven identical, cysteine-free subunits. A side view of the ribbon structure (PDB code 7AHL) is shown. One of the seven subunits is highlighted in magenta. (*B*) αHL pore embedded in a planar lipid bilayer for single-channel electrical recording. A cross section of P_C is shown. P_C contains one subunit (of seven) with a cysteine residue at position 137 (highlighted in *cyan* and labeled), which is located in the middle of the transmembrane β barrel with the side chain pointing toward the lumen. Four mutations (K8A, M113G, K131G, and K147G) were introduced into WT αHL by site-directed mutagenesis to create the AG background on which P_C is based. The locations of the four mutations are highlighted and indicated. Metal ions (Ag^+ or Cd^{2+}) were added to the *cis* compartment, which is the side where the cap domain of the αHL pore resides and is connected to ground. During measurements, a potential of –50 mV was applied to the *trans* compartment relative to the *cis* compartment.

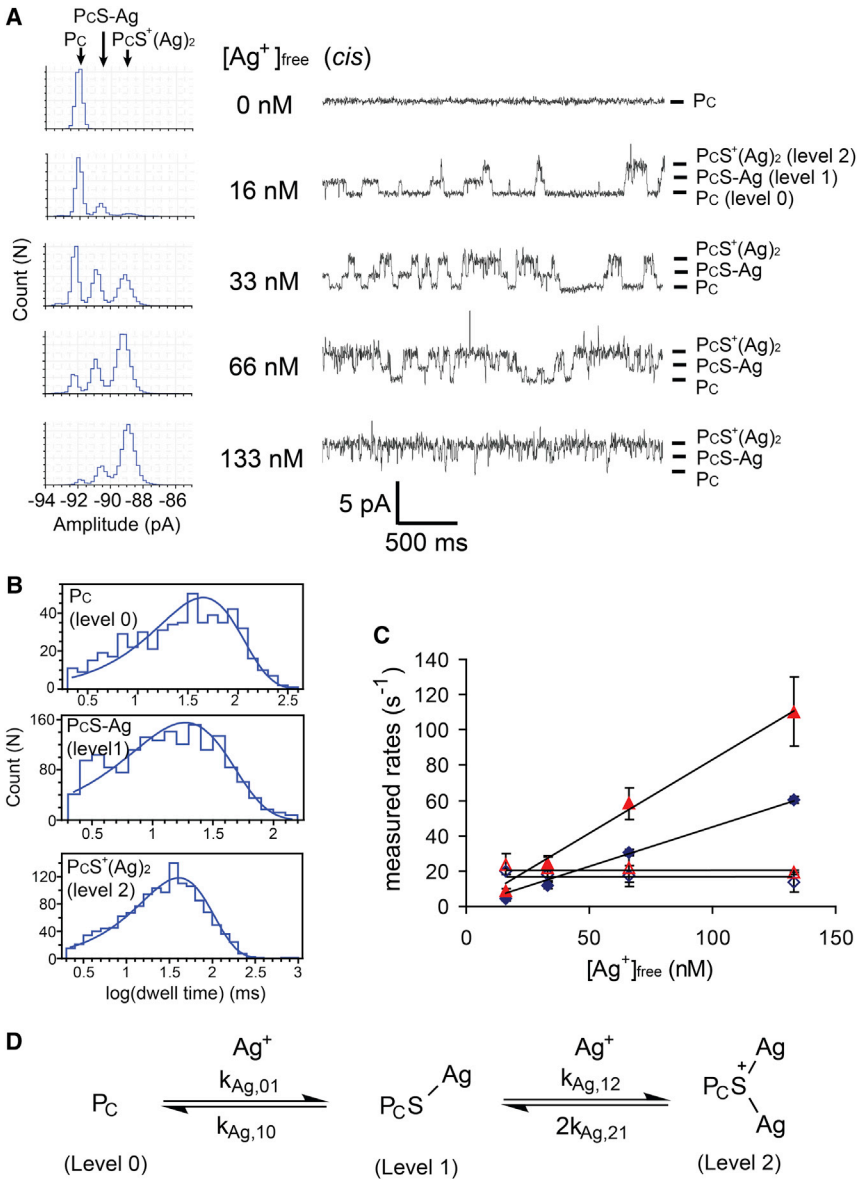

FIGURE 3 Reversible and sequential binding of two Ag^+ ions to a single cysteine residue. (*A*) Current recordings at different free Ag^+ ion concentrations, $[Ag^+]_{free}$ (Ag^+ was added as $AgNO_3$ to the *cis* compartment). Each current level is labeled on the right: P_C = unoccupied pore (level 0); P_CS-Ag = one Ag^+ ion-bound (level 1); $P_CS^+(Ag)_2$ = two Ag^+ ions-bound (level 2). All-points amplitude histograms are shown on the left. Conditions: 2 M KNO_3, 10 mM MOPS, 10 mM EDTA, pH 7.4, at 22°C and –50 mV. Under these conditions, P_C has an open pore current of –96 ± 2 pA (n = 5). (*B*) Dwell-time histograms for P_C, P_CS-Ag, and $P_CS^+(Ag)_2$ in the presence of 66 nM $[Ag^+]_{free}$. Each histogram was fitted to a single-exponential function using Clampfit (Molecular Devices) to determine the mean dwell time ($\bar{\tau}$). (*C*) Plots of the measured rates of each transition versus $[Ag^+]_{free}$. Each data point (mean ± SD) was obtained from three experiments: level 0→level 1 (*blue solid rhombus*), level 1→0 (*blue open rhombus*), level 1→2 (*red solid triangle*), level 2→1 (*red open triangle*). The determination of rate constants from these plots is described in the Materials and Methods section. (*D*) Kinetic scheme describing the sequential association of two Ag^+ ions with the cysteine side chain in P_C. Direct transitions between P_C and $P_CS^+(Ag)_2$ are not observed. This scheme was used in QuB (see Materials and Methods) for the determination of rate constants.

$k_{Ag,01}$ = (4.4 ± 0.3) × 10^8 $M^{-1}s^{-1}$ and $k_{Ag,12}$ = (8.3 ± 1.3) × 10^8 $M^{-1}s^{-1}$), whereas both 1→0 and 2→1 are independent of $[Ag^+]_{free}$: $v_{10} = k_{Ag,10}$ and $v_{21} = k_{Ag,21}$, where $k_{Ag,10}$ = 17 ± 1 s^{-1} and $k_{Ag,21}$ = 11 ± 3 s^{-1} (n = 3; Fig. 3 *D*). The first and second equilibrium dissociation constants calculated from these data are $K_{d,Ag,1} = k_{Ag,10}/k_{Ag,01}$ = (4.0 ± 0.5) × 10^{-8} M and $K_{d,Ag,2} = k_{Ag,21}/k_{Ag,12}$ = (1.3 ± 0.3) × 10^{-8} M (Table 1). The overall K_d for Ag^+ binding = $K_{d,Ag,1}.K_{d,Ag,2}$ = (5.3 ± 1.4) × 10^{-16} M^2.

Because a Ag^+ ion is involved in both the 0→1 and the 1→2 transitions, levels 1 and 2 are proposed to be P_C-S-Ag and $P_CS^+(Ag)_2$, respectively (Fig. 3 *D*). A thiolate sulfur atom can bridge two Ag^+ ions (28). Therefore, level 2 is believed to represent Ag-S^+(P_C)-Ag rather than P_C-S-Ag^+-Ag (with a bridging Ag), which is supported by the absence of direct transitions between $P_CS^+(Ag)_2$ and P_C (i.e., 2↔0 does not occur).

In addition to reversible Ag^+ binding, Ag^+-induced complete blockade of the P_C pore was frequently observed: 64% of experiments (87 out of 136) showed complete blockade within 10 min after the addition of a submicromolar concentration of free Ag^+ ion (Fig. 4, *A* and *B*). The blockade was usually stepwise and the process was completed <30 s after its initiation. Such blockades could be reversed by the addition of excess thiol (more than one equivalent of thiol compound relative to the total $AgNO_3$ added), such as DTT, cysteamine, or β-mercaptoethanol, to either the *cis* or *trans* compartment. Pore unblocking occurred in a single step (Fig. 4 *C*) or by a stepwise (Fig. 4 *D*) mechanism. Full blockade arose again if the concentration of thiol was diluted to ~100 nM. If ~100 nM thiol (e.g. cysteine,

TABLE 1 Association and dissociation rate constants, and equilibrium dissociation constants for Ag^+ and Cd^{2+} with the P_C, P_{HC}, and P_{CC} pores

	Mutant	Current blockade (ΔI) (pA)	Association rate constant ($M^{-1}s^{-1}$)	Dissociation rate constant (s^{-1})	Equilibrium dissociation constant (M)[e]
Ag^+	P_C[a] ($n = 3$)	1.6 ± 0.3	$k_{Ag,01}$[c] (4.4 ± 0.3) × 10^8	$k_{Ag,10}$[c] 17 ± 1	$K_{d,Ag,1}$ (4.0 ± 0.5) × 10^{-8}
		3.6 ± 0.6	$k_{Ag,12}$[c] (8.3 ± 1.3) × 10^8	$k_{Ag,21}$[c] 11 ± 3	$K_{d,Ag,2}$ (1.3 ± 0.3) × 10^{-8}
Cd^{2+}	P_C[b] ($n = 4$)	3.8 ± 0.1	$k_{Cd,01}$ (5.9 ± 0.6) × 10^4	$k_{Cd,10}$ 13 ± 1	$K_{d,Cd}$ (2.2 ± 0.4) × 10^{-4}
	P_{CC}[b] ($n = 3$)	1.4 ± 0.2	$k^{app}{}_{CC,01}$[d] (5.3 ± 1.8) × 10^4	$k^{app}{}_{CC,10}$[d] (3.5 ± 0.5) × 10^{-2}	$K^{app}{}_{d,CC}$ (6.5 ± 2.4) × 10^{-7}
	P_{HC}[b] ($n = 3$)	4.9 ± 0.6	$k^{app}{}_{HC,01}$[d] (1.3 ± 0.3) × 10^6	$k^{app}{}_{HC,10}$[d] 9.2 ± 2.5	$K^{app}{}_{d,HC}$ (6.8 ± 2.4) × 10^{-6}

Conditions for Ag^+: pH 7.4 (2 M KNO_3, 10 mM MOPS, 10 mM EDTA) at −50 mV and 22°C. Conditions for Cd^{2+}: pH 7.4 (2 M KNO_3, 10 mM MOPS, Chelex treated) at −50 mV and 22°C. Values (mean ± SD) were calculated by using the concentration of free Ag^+ ion or the total concentration of Cd^{2+} ion.
[a]P_C binds two Ag^+ ions.
[b]The association of Cd^{2+} to these mutants shows bimolecular kinetics with first-order dependencies on [Cd^{2+}]. Binding of a second Cd^{2+} is not observed.
[c]For definitions, see the kinetic schemes in Fig. 3 *D*.
[d]These values are the rate constants calculated directly from the experimental data (see Figs. 7 and 8). They can be resolved into the rate constants of individual steps. Refer to the Supporting Material for more details.
[e]The equilibrium dissociation constant equals the dissociation rate constant divided by the association rate constant from the same row of the table.

thioglycolate, and cysteamine) was present initially, the onset of the Ag^+ ion-induced current blockade took place with a shorter lag time while showing similar blocking characteristics (see Supporting Material). The complete blockade, with or without added thiol, usually begins from the single Ag(I)-bound state (P_C-S-Ag; see Fig. 4 *B*). Blockade did not occur with αHL $(AG)_7$, showing that a lumenal cysteine side chain is required. Because residual thiols from the protein preparation (thioglycolate, β-mercaptoethanol, and DTT, at the tens of nanomolar level) were present during planar lipid bilayer experiments, we propose that the blockade of P_C arises from the formation of Ag^+-thiol coordination polymers on the cysteine thiol group (29,30) (Fig. S2). Because Ag^+-thiol polymers form reversibly in solution (31), the addition of excess thiol breaks protein-bound polymers into shorter chains, which diffuse away, thereby unblocking the pore. Whether the unblocking process occurs as a single step (Fig. 4 *C*) or multiple steps (Fig. 4 *D*) depends on the initial site of polymer cleavage.

Implications for the use of Ag^+ in SCAM

In macroscopic studies of ion channels (e.g., the P2X purinoreceptor (32), Shaker K^+ channel (3), and cyclic nucleotide-gated (CNG) channel (33)), Ag^+ binds to exposed cysteine thiols with apparent bimolecular rate constants of up to 10^8 $M^{-1}s^{-1}$ (32). The binding is effectively

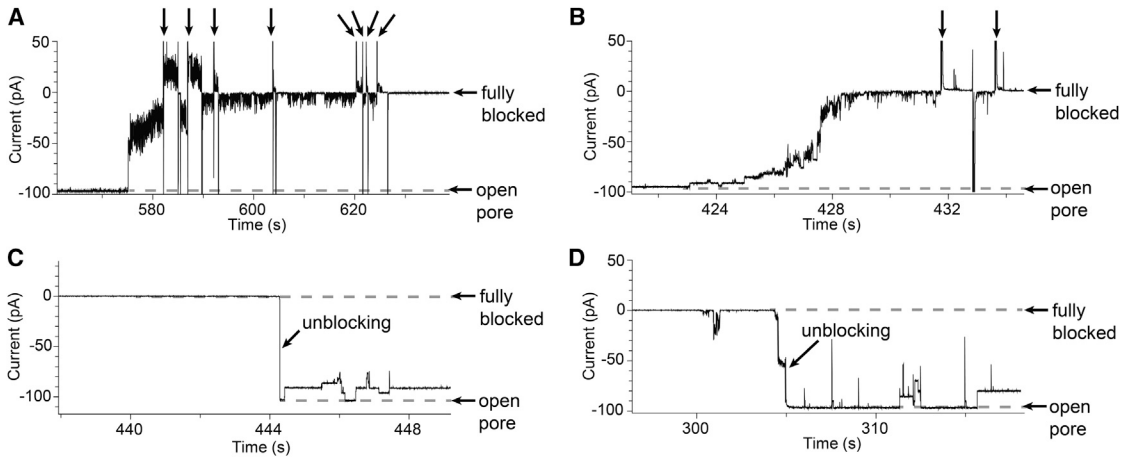

FIGURE 4 Complete blockade of P_C by $AgNO_3$. (*A* and *B*) Full blockade of P_C after the addition of $AgNO_3$ (*cis*, 33 nM free Ag^+ ion). Soon after the appearance of reversible Ag^+ ion binding events as shown in Fig. 3 *A*, P_C underwent a stepwise decrease in conductance, which eventually led to complete blockade (64% of experiments exhibited full blockade). The applied potential was switched to +50 mV as indicated by black arrows on the current traces. In *A*, a sudden large drop in conductance was first observed, followed by a stepwise decrease in conductance. In *B*, a stepwise decrease in conductance from the open pore level to the fully blocked level was seen. The noise in the intermediate levels may be caused by polymer movement (35,36). (*C* and *D*) Reopening of blocked P_C. After the full blockade induced by $AgNO_3$, cysteamine was added to the *cis* compartment. More than one equivalent of cysteamine (10 μM) relative to the total amount of $AgNO_3$ (*cis*, 8 μM) was necessary for unblocking. Cysteamine forms oligomers with Ag^+ ion in solution (37). The oligomers occasionally react with the protein cysteine residue, leading to additional incomplete blockades. Panels *C* and *D* show one-step and stepwise unblocking, respectively.

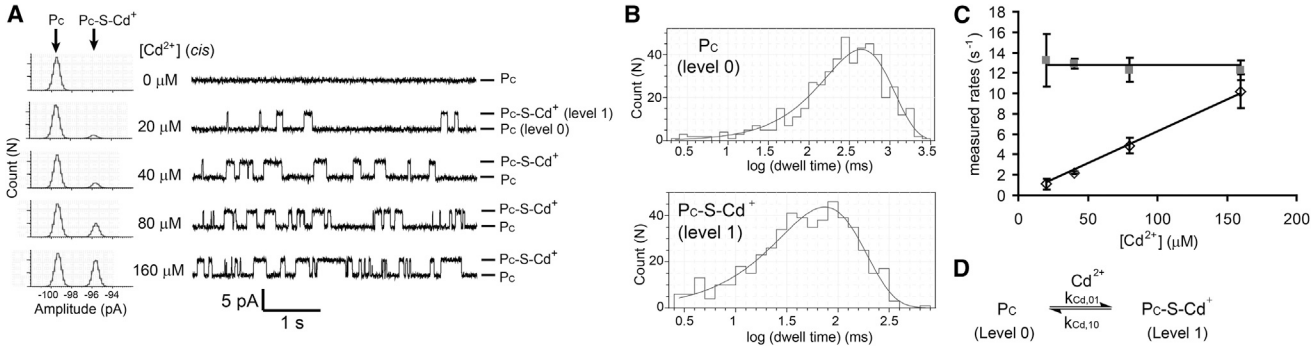

FIGURE 5 Reversible binding of Cd^{2+} ion to P_C. (*A*) Stacked current traces for P_C at different concentrations of $Cd(NO_3)_2$ ($[Cd^{2+}]$, *cis*). Each level is labeled on the right: P_C, open pore; $P_CS\text{-}Cd^+$, pore with Cd^{2+}-bound. All-points amplitude histograms are shown on the left. The histograms are fitted to the sum of two Gaussian functions. Conditions: 2 M KNO_3, 10 mM MOPS, treated with Chelex ion exchange resin, pH 7.4, at –50 mV and 22°C. (*B*) Dwell-time histograms of P_C and $P_CS\text{-}Cd^+$ in the presence of 40 μM $Cd(NO_3)_2$. Each histogram was fitted to a single-exponential function using Clampfit (Molecular Devices) to determine the mean dwell time ($\bar{\tau}$). (*C*) Plots of the measured rates of each transition (as the reciprocals of the mean dwell times for the open pore ($1/\bar{\tau}_{PC}$, *black open rhombus*) and the Cd^{2+}-occupied pore ($1/\bar{\tau}_{PCS\text{-}Cd^+}$, *gray solid square*)) versus $[Cd^{2+}]$. Each data point (mean ± SD) was obtained from four experiments. (*D*) Kinetic scheme describing the binding of Cd^{2+} to P_C.

irreversible because the removal of Ag^+ does not reverse the blockade over at least 5 s. Our association rate constants ($k_{Ag,01} = (4.4 \pm 0.3) \times 10^8\ M^{-1}s^{-1}$ and $k_{Ag,12} = (8.3 \pm 1.3) \times 10^8\ M^{-1}s^{-1}$ for P_C) are similar to the maximum rate constants observed in ion channel studies, consistent with the side chain of Cys-137 being water accessible. However, in contrast to the findings with ion channels, reversible coordination of two Ag^+ ions is observed in our single-molecule experiments. Because $k_{Ag,12} > k_{Ag,01}$, binding as measured in macroscopic current recordings would be described by a single exponential. Alternatively, the first Ag^+ ion might block the narrow conductive pathway of an ion channel completely, thereby producing a one-step bimolecular blockade. Finally, with regard to permanent blockade, it should be noted that most ion channels investigated by SCAM comprise more than one cysteine-containing subunit, and the coordination of Ag^+ by proximal thiol groups contributed by adjacent subunits or by the side chains of additional amino acids (e.g., histidine) might lead to irreversible obstruction of the conductive pathway.

Cd^{2+} binding

By contrast, Cd^{2+} (20–160 μM) added to P_C at –50 mV and pH 7.4 (2 M KNO_3, 10 mM MOPS) provoked reversible blockades with just one new level: $\Delta I = 3.8 \pm 0.1$ pA ($n = 4$; Fig. 5 *A*). The association of Cd^{2+} was bimolecular with $v_{01} = k_{Cd,01}[Cd^{2+}]$, where $k_{Cd,01} = (5.9 \pm 0.6) \times 10^4\ M^{-1}s^{-1}$, whereas dissociation was unimolecular with $v_{10} = k_{Cd,10}$, where $k_{Cd,10} = 13 \pm 1\ s^{-1}$ ($n = 4$; Fig. 5 *C*). Therefore, level 1 (Fig. 5 *A*) is assigned the structure $P_C\text{-}S\text{-}Cd^+$ (Fig. 5 *D*). The equilibrium dissociation constant is $K_{d,Cd} = k_{Cd,10}/k_{Cd,01} = (2.2 \pm 0.4) \times 10^{-4}$ M ($n = 4$; Table 1).

The binding of Cd^{2+} to cysteine side chains in ion channels is strengthened by the presence of additional coordinating ligands (5,32). To create such a chelation site in the αHL pore, an additional cysteine or histidine residue was introduced in the AG background at position 135, which is adjacent to Cys-137 on the same β strand (Fig. 6). The heteroheptameric pores formed with each of these two mutants were termed P_{CC} and P_{HC}. Single-molecule kinetic analysis showed that both P_{CC} and P_{HC} bind one Cd^{2+}, but do so more tightly than P_C (Table 1; Figs. 7 and 8). Apparent bimolecular association kinetics were observed. No half-liganded intermediates were seen, and therefore the second coordination step must be fast, which is in contrast to the binding of Zn^{2+} by an αHL pore equipped with two iminodiacetate

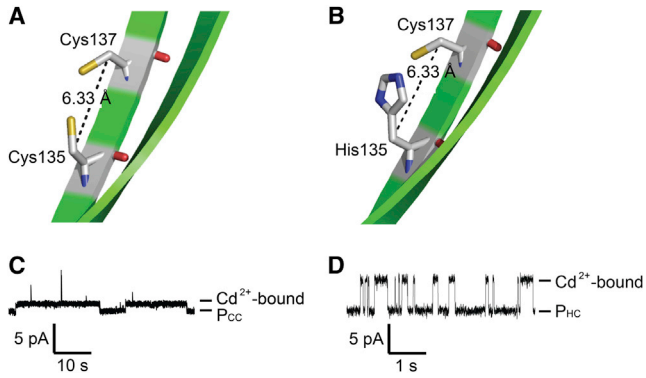

FIGURE 6 Chelation sites for Cd^{2+} within the αHL pore. (*A*) Cys-135/Cys-137 (P_{CC}). (*B*) His-135/Cys-137 (P_{HC}). Positions 135 and 137 are located on a transmembrane β strand of αHL (see Fig. 2); both have their amino acid side chains pointing toward the pore lumen. The Cβ–Cβ distance between positions 135 and 137 is 6.3 Å (11). The orientations of the Cβ-S and Cβ-imidazole bonds are for illustration purposes only. The two antiparallel β strands of one αHL protomer are shown. (*C* and *D*) Current recordings showing the reversible association of Cd^{2+} with (*C*) P_{CC} and (*D*) P_{HC} at 5 μM $Cd(NO_3)_2$ (*cis*). Note that the time bar in *C* is 10 times longer than that in *D*.

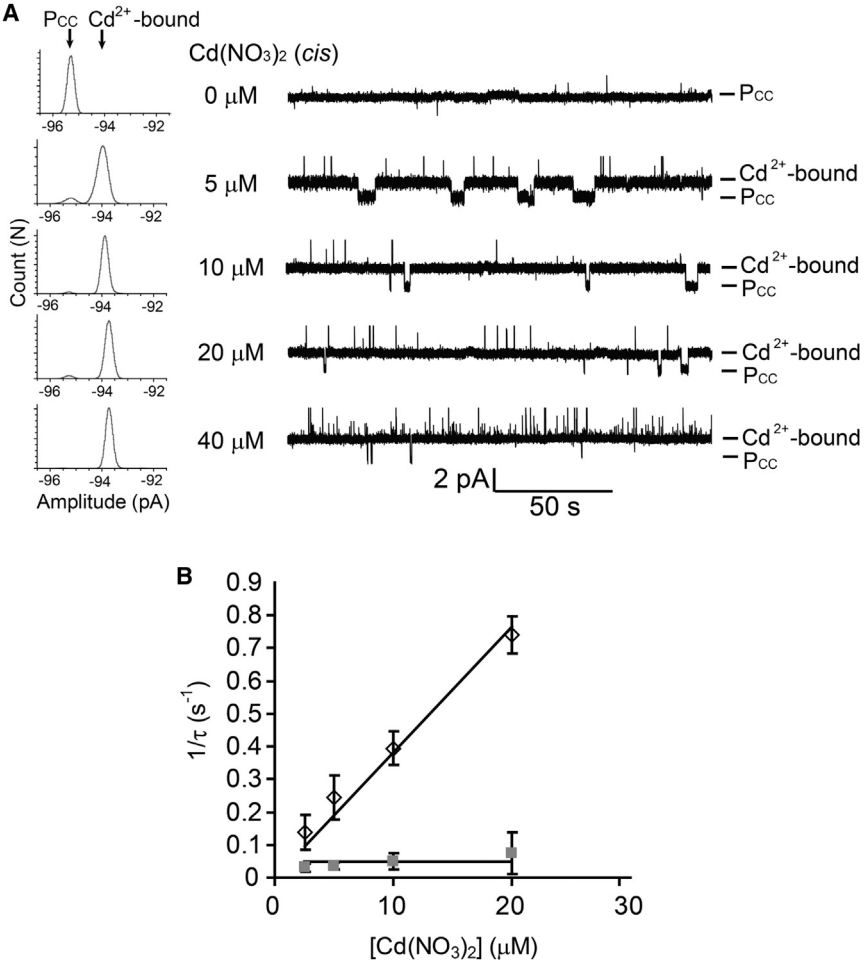

FIGURE 7 Reversible binding of Cd^{2+} to P_{CC}. (*A*) Stacked current recording traces of P_{CC}, $(AG)_6(L135C/G137C\text{-}AG)_1$, at various concentrations of $Cd(NO_3)_2$ (*cis*), as labeled on the left of the traces. The conditions were the same as in Fig. 5. Only two current levels were observed, namely, the open pore (P_{CC}) and the pore with Cd^{2+} bound, as labeled on the right of the traces. All-points amplitude histograms are shown to the far left. The histograms are fitted to the sum of two Gaussian functions. (*B*) Reciprocals of the mean dwell times for the unoccupied pore ($1/\overline{\tau}_{PCC}$, *black open rhombus*) and the pore with bound Cd^{2+} ($1/\overline{\tau}_{Cd^{2+}\text{-bound}}$, *gray solid square*) versus the concentration of $Cd(NO_3)_2$. Each data point is the mean ± SD from three repeats. The association and dissociation of Cd^{2+} follow simple bimolecular and unimolecular kinetics, respectively. The binding of a second Cd^{2+} is not observed.

ligands (14). The coordination of a second Cd^{2+} ion was not detected.

Compared with P_C, Cd^{2+} shows 22 times faster association with P_{HC} ($k^{app}_{HC,01} = (1.3 \pm 0.3) \times 10^6\ M^{-1}s^{-1}$) and 370 times slower dissociation from P_{CC} ($k^{app}_{CC,10} = (3.5 \pm 0.5) \times 10^{-2}\ s^{-1}$) (Table 1). Dissociation from P_{HC} ($k^{app}_{HC,10} = 9.2 \pm 2.5\ s^{-1}$) and association with P_{CC} ($k_{CC,01} = (5.3 \pm 1.8) \times 10^4\ M^{-1}s^{-1}$) have rate constants similar to the corresponding values for P_C. The increased apparent association rate constant for P_{HC} may arise either from the lowering of the pK_a of Cys-137 by the adjacent imidazole ring to favor the reactive thiolate or from the rapid initial coordination of Cd^{2+} by the imidazole ring (for discussion, see Supporting Material). The decreased apparent dissociation rate constant for P_{CC} results either from the rapid coordination of Cd^{2+} bound to a first thiol by the second protein thiol or from the slow cleavage of the first Cd-S bond in the fully coordinated complex (see Supporting Material). These chelate effects lead to a 30-fold tighter binding of Cd^{2+} to P_{HC} ($K_{d,HC} = (6.8 \pm 2.4) \times 10^{-6}$ M) and 300-fold tighter binding to P_{CC} ($K_{d,CC} = (6.5 \pm 2.4) \times 10^{-7}$ M) compared with P_C. The K_d values and the increase in binding affinity by an additional Cys or His ligand are in agreement with previous findings obtained with β-strand or α-helical peptides (34).

CONCLUSIONS

The rate of modification of cysteine residues by thiophilic reagents is the primary readout obtained from SCAM. The correct interpretation of these data, which relies on an understanding of the modification reactions, is therefore pivotal for deciphering the topology of ion channels in different conformations. In this work, we determined the coordination stoichiometries and kinetics of the two most important metal ion probes, Ag^+ and Cd^{2+}, with respect to cysteine thiol groups at the single-molecule level, and established the αHL pore as a platform on which new reagents can be tested. We also hope that our findings will guide single-molecule studies of ion channels with thiophilic metal ions, which could provide better structural information than macroscopic studies. Our findings suggest that Cd^{2+}, which binds to thiols in a simple bimolecular fashion, and for which neighboring Cys and His residues have predictable effects, might be the metal ion of choice for such work.

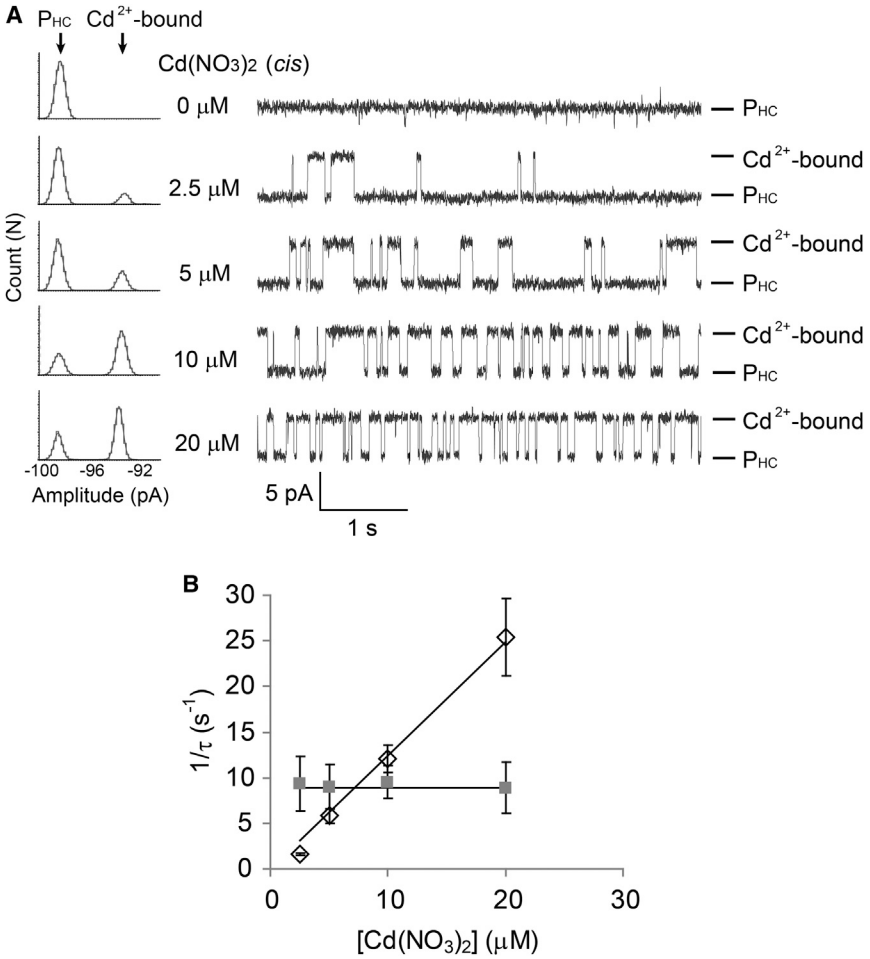

FIGURE 8 Reversible binding of Cd^{2+} to P_{HC}. (*A*) Stacked current recording traces of P_{HC}, $(AG)_6(L135H/G137C\text{-}AG)_1$, at various concentrations of $Cd(NO_3)_2$ (*cis*) as labeled on the left of the traces. The conditions were the same as in Fig. 5. Only two levels were observed, namely, the open pore (P_{HC}) and a level with bound Cd^{2+}, as indicated on the right of the traces. All-points amplitude histograms are shown to the far left. The histograms are fitted to the sum of two Gaussian functions. (*B*) Reciprocals of the mean dwell times of the unoccupied pore ($1/\overline{\tau}_{PHC}$, *black open rhombus*) and the pore with bound Cd^{2+} ($1/\overline{\tau}_{Cd^{2+}\text{-bound}}$, *gray solid square*) versus the concentration of $Cd(NO_3)_2$. Each data point is the mean ± SD from three repeats. The association of Cd^{2+} with P_{HC} demonstrates simple bimolecular kinetics with a first-order dependence on $[Cd^{2+}]$, whereas the dissociation is unimolecular and independent of $[Cd^{2+}]$. The binding of a second Cd^{2+} is not observed.

SUPPORTING MATERIAL

Supporting analysis including figures, equations, and references (38-41) are available at http://www.biophysj.org/biophysj/supplemental/S0006-3495(13)00514-6.

We thank Dr. Lajos Höfler for help with the noise analysis. This work was supported by a European Research Council Advanced Grant and Oxford Nanopore Technologies. Lai-Sheung Choi was the recipient of a University of Oxford Croucher Scholarship. Hagan Bayley is the founder, a director, and a shareholder of Oxford Nanopore Technologies.

REFERENCES

1. Karlin, A., and M. H. Akabas. 1998. Substituted-cysteine accessibility method. *Methods Enzymol.* 293:123–145.
2. Vinothkumar, K. R., and R. Henderson. 2010. Structures of membrane proteins. *Q. Rev. Biophys.* 43:65–158.
3. Lü, Q., and C. Miller. 1995. Silver as a probe of pore-forming residues in a potassium channel. *Science.* 268:304–307.
4. Pérez-García, M. T., N. Chiamvimonvat, …, G. F. Tomaselli. 1996. Structure of the sodium channel pore revealed by serial cysteine mutagenesis. *Proc. Natl. Acad. Sci. USA.* 93:300–304.
5. Webster, S. M., D. Del Camino, …, G. Yellen. 2004. Intracellular gate opening in Shaker K^+ channels defined by high-affinity metal bridges. *Nature.* 428:864–868.
6. Preston, G. M., J. S. Jung, …, P. Agre. 1993. The mercury-sensitive residue at cysteine 189 in the CHIP28 water channel. *J. Biol. Chem.* 268:17–20.
7. Akabas, M. H., D. A. Stauffer, …, A. Karlin. 1992. Acetylcholine receptor channel structure probed in cysteine-substitution mutants. *Science.* 258:307–310.
8. Shannon, R. D. 1976. Revised effective ionic radii and systematic studies of interatomic distances in halides and chalcogenides. *Acta Crystallogr. A.* 32:751–767.
9. Lincoln, S. F., D. T. Richens, and A. G. Sykes. 2004. Metal aqua ions. *In* Comprehensive Coordination Chemistry. II: From Biology to Nanotechnology, Vol. 1. A. B. P. Lever, J. A. McCleverty, and T. J. Meyer, editors.. Elsevier, Amsterdam/Oxford. 515–556.
10. Holmgren, M., K. S. Shin, and G. Yellen. 1998. The activation gate of a voltage-gated K^+ channel can be trapped in the open state by an intersubunit metal bridge. *Neuron.* 21:617–621.
11. Song, L., M. R. Hobaugh, …, J. E. Gouaux. 1996. Structure of staphylococcal α-hemolysin, a heptameric transmembrane pore. *Science.* 274:1859–1866.
12. Bayley, H., T. Luchian, …, M. B. Steffensen. 2008. Single-molecule covalent chemistry in a protein nanoreactor. *In* Single Molecules and Nanotechnology. R. Rigler and H. Vogel, editors.. Springer, Heidelberg. 251–277.
13. Braha, O., L.-Q. Gu, …, H. Bayley. 2000. Simultaneous stochastic sensing of divalent metal ions. *Nat. Biotechnol.* 18:1005–1007.

14. Hammerstein, A. F., S.-H. Shin, and H. Bayley. 2010. Single-molecule kinetics of two-step divalent cation chelation. *Angew. Chem. Int. Ed. Engl.* 49:5085–5090.

15. Walker, B., M. Krishnasastry, …, H. Bayley. 1992. Functional expression of the α-hemolysin of *Staphylococcus aureus* in intact *Escherichia coli* and in cell lysates. Deletion of five C-terminal amino acids selectively impairs hemolytic activity. *J. Biol. Chem.* 267:10902–10909.

16. Shin, S.-H., M. B. Steffensen, …, H. Bayley. 2007. Formation of a chiral center and pyrimidal inversion at the single-molecule level. *Angew. Chem. Int. Ed. Engl.* 46:7412–7416.

17. Wolfe, A. J., M. M. Mohammad, …, L. Movileanu. 2007. Catalyzing the translocation of polypeptides through attractive interactions. *J. Am. Chem. Soc.* 129:14034–14041.

18. Choi, L.-S., and H. Bayley. 2012. *S*-nitrosothiol chemistry at the single-molecule level. *Angew. Chem. Int. Ed. Engl.* 51:7972–7976.

19. Shin, S.-H., T. Luchian, S. Cheley, O. Braha, and H. Bayley. 2002. Kinetics of a reversible covalent-bond-forming reaction observed at the single molecule level. *Angew. Chem. Int. Ed. Engl.* 41:3707–3709, 3523.

20. Lu, S., W.-W. Li, …, H. Bayley. 2010. A primary hydrogen-deuterium isotope effect observed at the single-molecule level. *Nat. Chem.* 2:921–928.

21. Reference deleted in proof.

22. Martell, A. E., and R. M. Smith. 1974. Critical Stability Constants. Plenum Press, New York/London.

23. Vivaudou, M. B., C. Arnoult, and M. Villaz. 1991. Skeletal muscle ATP-sensitive K^+ channels recorded from sarcolemmal blebs of split fibers: ATP inhibition is reduced by magnesium and ADP. *J. Membr. Biol.* 122:165–175.

24. Gruen, L. C. 1975. Interaction of amino acids with silver(I) ions. *Biochim. Biophys. Acta.* 386:270–274.

25. Lee, V. W.-M., H. Li, …, K. W. M. Siu. 1998. Relative silver(I) ion binding energies of α-amino acids: a determination by means of the kinetic method. *J. Am. Soc. Mass Spectrom.* 9:760–766.

26. Shoeib, T., K. W. M. Siu, and A. C. Hopkinson. 2002. Silver ion binding energies of amino acids: use of theory to assess the validity of experimental silver ion basicities obtained from the kinetic method. *J. Phys. Chem. A.* 106:6121–6128.

27. Jover, J., R. Bosque, and J. Sales. 2008. A comparison of the binding affinity of the common amino acids with different metal cations. *Dalton Trans.* 45:6441–6453.

28. Dance, I. G., L. J. Fitzpatrick, …, M. L. Scudder. 1983. The intertwined double-(-Ag-SR-)$_\infty$-strand chain structure of crystalline (3-methylpentane-3-thiolato)silver, in reaction to $(AgSR)_8$ molecules in solution. *Inorg. Chem.* 22:3785–3788.

29. Nan, J., and X.-P. Yan. 2010. A circular dichroism probe for L-cysteine based on the self-assembly of chiral complex nanoparticles. *Chemistry.* 16:423–427.

30. Shen, J.-S., D.-H. Li, …, Y. B. Jiang. 2011. Metal-metal-interaction-facilitated coordination polymer as a sensing ensemble: a case study for cysteine sensing. *Langmuir.* 27:481–486.

31. Shen, J.-S., D.-H. Li, …, Y.-B. Jiang. 2009. Highly selective iodide-responsive gel-sol state transition in supramolecular hydrogels. *J. Mater. Chem.* 19:6219–6224.

32. Li, M., T. Kawate, S. D. Silberberg, and K. J. Swartz. 2010. Pore-opening mechanism in trimeric P2X receptor channels. *Nat. Commun.* 1:44.

33. Flynn, G. E., and W. N. Zagotta. 2001. Conformational changes in S6 coupled to the opening of cyclic nucleotide-gated channels. *Neuron.* 30:689–698.

34. Puljung, M. C., and W. N. Zagotta. 2011. Labeling of specific cysteines in proteins using reversible metal protection. *Biophys. J.* 100:2513–2521.

35. Movileanu, L., S. Howorka, …, H. Bayley. 2000. Detecting protein analytes that modulate transmembrane movement of a polymer chain within a single protein pore. *Nat. Biotechnol.* 18:1091–1095.

36. Shin, S.-H., and H. Bayley. 2005. Stepwise growth of a single polymer chain. *J. Am. Chem. Soc.* 127:10462–10463.

37. Andersson, L.-O. 1972. Study of some silver-thiol complexes and polymers: stoichiometry and optical effects. *J. Polym. Sci. A1.* 10: 1963–1973.

38. Greenwood, N. N., and A. Earnshaw. 1984. Chemistry of the Elements. Pergamon Press, New York.

39. Colquhoun, D., and A. G. Hawkes. 2009. The principles of the stochastic interpretation of ion-channel mechanisms. *In* Single-Channel Recording. B. Sakmann and E. Nehre, editors. Springer, New York/London. pp. 397–482.

40. DeFelice, L. J. 1981. Introduction to Membrane Noise. Plenum Press, New York.

41. Verveen, A. A., and L. J. DeFelice. 1974. Membrane noise. *Prog. Biophys. Mol. Biol.* 28:189–265.

submitted to BIOPHYSICAL JOURNAL (REGULAR ARTICLE)

Supporting Material

Rates and stoichiometries of metal ion probes of cysteine residues within ion channels

Lai-Sheung Choi, Tivadar Mach and Hagan Bayley[1]

Department of Chemistry, University of Oxford, Oxford, OX1 3TA, United Kingdom

[1] To whom correspondence should be addressed. Address: Department of Chemistry, University of Oxford, Oxford, OX1 3TA, United Kingdom. Phone: +44 1865 285101. Fax: +44 1865 275708. E-mail: hagan.bayley@chem.ox.ac.uk

SUPPORTING MATERIAL

1. Properties of the αHL AG mutant

By contrast with the weak anion selectivity of $(WT)_7$, $(AG)_7$ is cation-selective (the charge selectivity ratio P_{K^+}/P_{Cl^-} is 0.54 for $(WT)_7$ and 3.12 for $(AG)_7$ in 100 mM KCl (*cis*)/ 1 M KCl (*trans*), pH 7.4). The conductance of $(AG)_7$ (2.73 ± 0.01 nS in 2 M KCl, –50 mV) is about 1.5 times higher than that of $(WT)_7$ (1.78 ± 0.01 nS). AG shows comparable hemolytic activity to WT αHL.

2. Additional information on the complete blockade of P_C produced by Ag^+ ion

To determine whether the full blockade of P_C (see Fig. 4) arises from Ag^+-thiol polymer formation, we tried to remove residual thiol from the protein preparation. Thiols, including thioglycolate, β-mercaptoethanol and DTT, were added to provide a reducing environment during protein preparation and for protein storage. Tens of nM of thiols remained in the chamber during planar lipid bilayer experiments. Buffer replacement in the bilayer apparatus was performed in attempts to reduce the thiols to pM concentrations, but pore blockade still occurred soon after Ag^+ addition. Replacing the thiols with tris(2-carboxylethyl)phosphine (TCEP) yielded P_C with an unreactive cysteine thiol.

We tested Ag^+-thiol polymer formation by the addition of different thiols to P_C in the presence of Ag^+. L-Cysteine, cysteamine and thioglycolate caused stepwise current reductions (Fig. S1) similar to the Ag^+-induced blockade shown in Fig. 4. The blockade began from the single Ag(I)-bound state (P_C-S-Ag), no matter which thiol was used. This reflects the role of Ag^+ in initiating polymer formation.

Other metal ions, for example Cd^{2+}, Ni^{2+}, Pb^{2+} and Hg^{2+}, do not cause a full blockade of P_C. Colloidal silver (Ag^0) formation by light-driven reduction (1) was avoided by keeping the bilayer chamber in the dark. The thiol compounds used also do not reduce Ag^+ ion. High quality reagents obtained from two suppliers were used to exclude impurities as a possible source of blockade.

Taking together the experimental findings presented in the main text [1. the unblocking of the pore by the addition of excess thiol (>1 equivalent of thiol relative to the total $AgNO_3$ added; 2. the shorter lag time for blocking in

the presence of added thiol (~100 nM, which is similar to the amount of free Ag^+); and, 3. the absence of blockade with the cysteine-free αHL $(AG)_7$ pore], we believe that the blockade of P_C is caused by Ag^+-thiol polymer formation initiated at the cysteine thiol group in the lumen of the pore (Fig. S2). Such polymer formation is expected to be very sensitive to trace amounts of thiols present in solution (2–5).

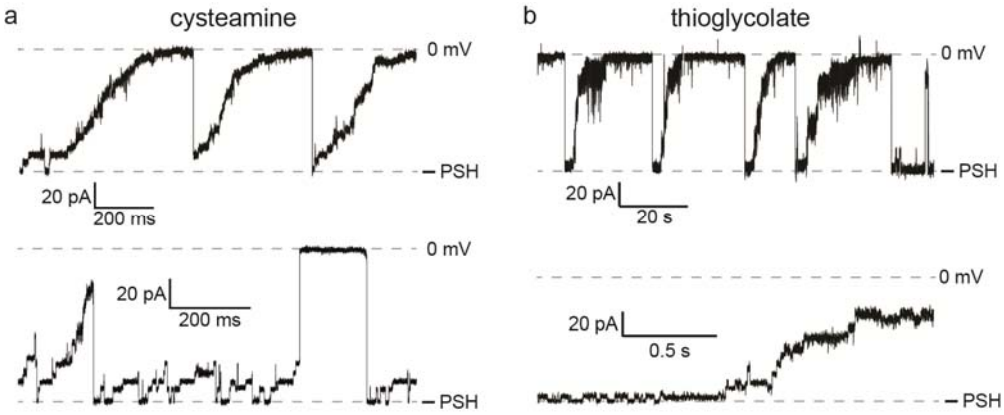

Figure S1. Silver(I)-thiol polymer formation in P_C. (*A*) Stepwise polymer formation with cysteamine. The two traces were collected under the same conditions. They show the stepwise build-up of different lengths of polymer that lead to different extents of pore blockade. The polymers always break in a single step, presumably by cleavage of the polymer chain near the cysteine residue of the pore (see Fig. S2). Conditions: 133 nM free Ag^+ (cis)/16 μM cysteamine (trans). (*B*) Stepwise polymer formation with thioglycolate. The lower trace shows a region of the upper trace with an expanded time axis. As in (*A*), polymers of different lengths were observed. Conditions: 266 nM free Ag^+ (cis)/1 μM thioglycolate (trans). L-Cysteine produces current blockades similar to those of thioglycolate. Irreversible pore blockade is observed in the absence of added thiol (see Fig. 4 in the main text). By contrast, the reversible blockades in (*A*) and (*B*) arise from the much higher concentration of thiol present, which promote polymer breakdown.

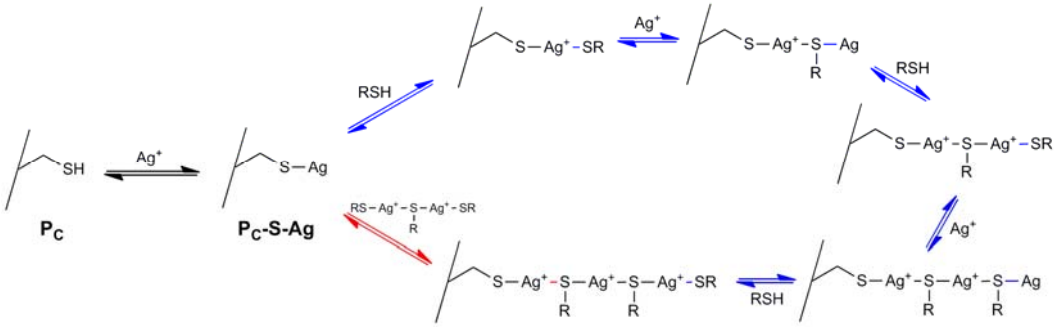

Figure S2. Proposed mechanisms for the growth and breakdown of silver(I)-thiol polymer on P_C. The alternating addition (or dissociation) of Ag^+ ion and thiol molecules (RSH) (black and blue arrows) leads to stepwise polymer growth (or breakdown). Sometimes the silver(I)-thiol polymer is preformed in solution. Its attachment (red arrow) leads to a one-step blockade as seen in Fig. 4*A* in the main text. One-step dissociation of the silver(I)-thiol polymer can also occur, and might be assisted by free thiol molecules. For simplicity, silver-thiol oligomers containing up to three Ag^+ ions are drawn. Longer polymers are possible. In addition to the thiol sulfur atom, carboxyl or amino group from the thiol compound can also coordinate to silver(I).

3. Binding of Cd^{2+} ion by P_{CC}

Our experimental results summarized in Table 1 in the main text show that 1) P_{CC} and P_C have similar Cd^{2+} association rate constants, while 2) the dissociation rate constant of P_{CC} is 370-times lower than that of P_C. The Cd^{2+} binding events displayed in Fig. 7*A* must be contributed by the species shown in the box in the following kinetic scheme. Because there is only one current level with Cd^{2+} bound, we suggest that it represents 2, which is implicit in the analysis that follows.

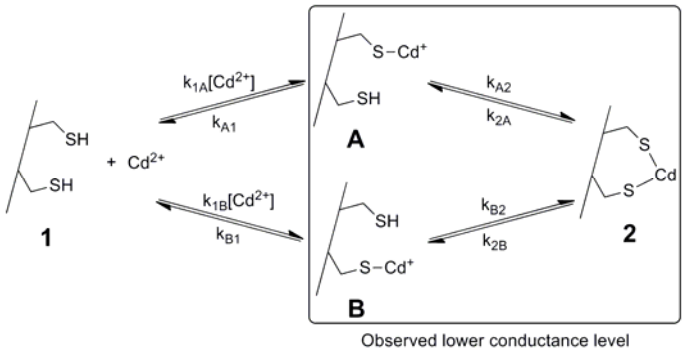

The probabilities of existence for each of the three species in the box are (6):

$$p_2 = \frac{k_{A2}k_{B2}}{k_{A2}k_{B2} + k_{2A}k_{B2} + k_{A2}k_{2B}} \quad \text{..... [1]}$$

$$p_A = \frac{k_{2A}k_{B2}}{k_{A2}k_{B2} + k_{2A}k_{B2} + k_{A2}k_{2B}} \quad \text{..... [2]}$$

$$p_B = \frac{k_{A2}k_{2B}}{k_{A2}k_{B2} + k_{2A}k_{B2} + k_{A2}k_{2B}} \quad \text{..... [3]}$$

where $p_2 + p_A + p_B = 1$

The apparent Cd^{2+} dissociation rate constant $k^{app}_{CC,10}$ (Table 1 in the main text) is:

$$k^{app}_{CC,10} = k_{A1}p_A + k_{B1}p_B$$

and substituting Eq. 2 and Eq. 3:

$$k_{CC,10}^{app} = \frac{k_{A1}k_{2A}k_{B2} + k_{B1}k_{A2}k_{2B}}{k_{A2}k_{B2} + k_{2A}k_{B2} + k_{A2}k_{2B}} \quad \text{[4]}$$

Therefore, the mean lifetime in the box is:

$$\left(\overline{\tau_2}\right) = \frac{k_{A2}k_{B2} + k_{2A}k_{B2} + k_{A2}k_{2B}}{k_{A1}k_{2A}k_{B2} + k_{B1}k_{A2}k_{2B}} \quad \text{[5]}$$

The lifetime outside the box is:

$$\left(\overline{\tau_1}\right) = \frac{1}{\left(\left(k_{1A} + k_{1B}\right)\left[Cd^{2+}\right]\right)} = \frac{1}{\left(k_{CC,01}^{app}\left[Cd^{2+}\right]\right)} \quad \text{[6]}$$

where $k^{app}_{CC,01}$ is the apparent association rate constant (Table 1).

If we assume that the two cysteine thiol groups have the same association and dissociation rate constants for Cd^{2+}, e.g. $k_{1A} = k_{1B}$, $k_{2A} = k_{2B}$ etc., Eq. 5 and Eq. 6 simplify to:

$$\overline{\tau_2} = \frac{1}{k_{A1}}\left(1 + \frac{k_{A2}}{2k_{2A}}\right) = \frac{1}{k_{CC,10}^{app}} \quad \text{[7]}$$

$$\overline{\tau_1} = \frac{1}{2k_{1A}\left[Cd^{2+}\right]} = \frac{1}{k_{CC,01}^{app}\left[Cd^{2+}\right]} \quad \text{[8]}$$

Further, the overall dissociation equilibrium constant ($K_{d,CC}$) for the chelation of Cd^{2+} is:

$$K_{d,CC} = \frac{k_{A1}k_{2A}}{k_{1A}k_{A2}} = K_{d,A}K_{d,2} \quad \text{[9]}$$

where $K_{d,A}$ (= k_{A1}/k_{1A}) and $K_{d,2}$ (= k_{2A}/k_{A2}) are the equilibrium dissociation constants of the first and second binding steps, respectively.

The apparent dissociation constant (Table 1) refers to the equilibrium between “inside” and “outside” the box (the low and high conductance states):

$$K_{d,CC}^{app} = \frac{\overline{\tau_1}[Cd^{2+}]}{\overline{\tau_2}} = \frac{k_{A1}k_{2A}}{k_{1A}(2k_{2A} + k_{A2})}$$

$K^{app}_{d,CC}$ reduces to $K_{d,CC}$ if $k_{2A} << k_{A2}$.

By using Eq. 8, $k_{1A} = k^{app}_{CC,01}/2 = (2.7 \pm 0.9) \times 10^4\ M^{-1}s^{-1}$.

By using k_{1A} and the value of $k_{Cd,10}$ for P_C (Table 1) as k_{A1}:

$$K_{d,A} = k_{A1}/k_{1A} = (4.8 \pm 1.7) \times 10^{-4}\ M$$

By substituting the same value for k_{A1} into Eq. 7 and using the apparent rate constant $k^{app}_{CC,10}$, we find:

$$K_{d,2} = k_{2A}/k_{A2} = (1.3 \pm 0.2) \times 10^{-3}$$

and the overall dissociation constant for 2, the fully coordinated Cd^{2+} complex:

$$K_{d,CC} = (6.6 \pm 2.6) \times 10^{-7}\ M$$

The $K_{d,CC}$ value is similar to the apparent dissociation constant $K^{app}_{d,CC}$ for the same P_{CC} pore (Table 1), and is over 300 times lower than $K_{d,Cd}$ for P_C, the pore containing a single cysteine. The lower overall dissociation constant for P_{CC} is due to the stability of the complex when Cd^{2+} is coordinated by both cysteines ($k_{2A} << k_{A2}$), and not by a higher association rate constant for Cd^{2+}.

4. Binding of Cd^{2+} ion by P_{HC}

Noise analysis with the histidine-only mutant P_H, i.e. $(AG)_6(L135H\text{-}AG)_1$ (see Fig. S3), shows that Cd^{2+} undergoes fast association and dissociation kinetics with the imidazole group. The residence time of Cd^{2+} on P_H is very short, hence the P_H-Cd^{2+} complex is not represented by a distinct time-resolved current level. Therefore, P_{HC} is analysed with H in the scheme below (P_{HC} with Cd^{2+} bound to His only) having the same conductance as the metal-free P_{HC}, 1. The observed binding events (Fig. 8*A*) presumably arise from the structures in the box:

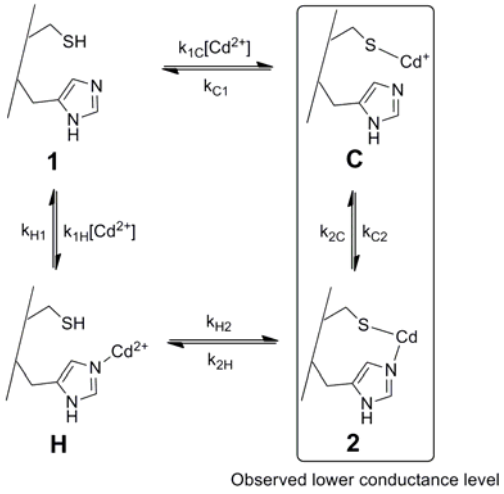

Our experimental results (Table 1 in the main text) show that 1) the association rate constant of Cd^{2+} with P_{HC} is 22-fold larger than that with P_C and 2) the dissociation rate constants of Cd^{2+} from P_C and P_{HC} are similar.

Considering the equilibrium in the box, the probabilities of finding C or 2 in the box are:

$$p_C = \frac{k_{2C}}{k_{2C} + k_{C2}} \quad \text{.....[10]}$$

$$p_2 = \frac{k_{C2}}{k_{2C} + k_{C2}} \quad \text{.....[11]}$$

such that $p_c + p_2 = 1$.

For moving out of the box, the apparent dissociation rate constant $k^{app}_{HC,10}$ (see Table 1):

$$k^{app}_{HC,10} = k_{C1}p_C + k_{2H}p_2$$

Substitution of Eq. 10 and Eq. 11 gives:

$$k^{app}_{HC,10} = \frac{k_{C1}k_{2C} + k_{2H}k_{C2}}{k_{2C} + k_{C2}} \quad \text{.....[12]}$$

The lifetime in the box is therefore:

$$\overline{\tau}_2 = \frac{1}{k^{app}_{HC,10}} = \frac{k_{2C} + k_{C2}}{k_{C1}k_{2C} + k_{2H}k_{C2}} \quad \text{.....[13]}$$

If $k_{2C} >> k_{C2}$ and $k_{C1}k_{2C} >> k_{2H}k_{C2}$, then $\overline{\tau}_2 = 1/k_{C1}$. If $k_{C2} >> k_{2C}$ and in the case that $k_{C1}k_{2C} << k_{2H}k_{C2}$, then $\overline{\tau}_2 = 1/k_{2H}$. The similar dissociation rate constants for Cd^{2+} from P_{HC} and P_C (Table 1), suggest that the first case may operate, although k_{2H} may, by coincidence, have similar value to the dissociation rate constant ($k_{Cd,10}$) of P_C.

Considering the two species outside the box, the probabilities of finding 1 and H are:

$$p_1 = \frac{k_{H1}}{\left(k_{H1} + k_{1H}\left[Cd^{2+}\right]\right)} \quad \text{.....[14]}$$

$$p_H = \frac{k_{1H}\left[Cd^{2+}\right]}{\left(k_{H1} + k_{1H}\left[Cd^{2+}\right]\right)} \quad \text{.....[15]}$$

such that $p_H + p_1 = 1$.

For moving into the box, the association rate v_{assoc} is:

$$v_{assoc} = k_{1C}\left[Cd^{2+}\right]p_1 + k_{H2}p_H$$

Substituting Eq. 14 and Eq. 15 gives:

$$v_{assoc} = \frac{(k_{1C}k_{H1} + k_{H2}k_{1H})[Cd^{2+}]}{(k_{H1} + k_{1H}[Cd^{2+}])} \quad \text{.....[16]}$$

Therefore, the lifetime outside the box is:

$$\bar{\tau}_1 = \frac{1}{v_{assoc}} = \frac{k_{H1} + k_{1H}[Cd^{2+}])}{(k_{1C}k_{H1} + k_{H2}k_{1H})[Cd^{2+}]} \quad \text{.....[17]}$$

With our experimental values of $k_{H1} \sim k_{H,10} = (2.5 \pm 0.4) \times 10^4$ s^{-1}, $k_{1H} \sim k_{H,01} = (2.2 \pm 0.1) \times 10^6$ $M^{-1}s^{-1}$ (see Fig. S3) and the maximum $[Cd^{2+}] = 20$ μM, $k_{H1} >> k_{1H}[Cd^{2+}]$, and Eq. 17 can be simplified to:

$$\bar{\tau}_1 = \frac{1}{v_{assoc}} = \frac{k_{H1}}{(k_{1C}k_{H1} + k_{H2}k_{1H})[Cd^{2+}]} \quad \text{.....[18]}$$

which supports the observed first-order $[Cd^{2+}]$-dependence of $1/\bar{\tau}_1$ (represented by $1/\bar{\tau}_{PHC}$ in Fig. 8*B*).

So in the experimental $[Cd^{2+}]$ range of 5–20 μM, the apparent association rate is:

$$k^{app}_{HC,01} = \frac{(k_{1C}k_{H1} + k_{H2}k_{1H})}{k_{H1}} \quad \text{.....[19]}$$

In one limiting case, association is primarily to form C, i.e. $k_{1C}k_{H1} >> k_{1H}k_{H2}$, and $k^{app}_{HC,01} \sim k_{1C}$. Because $k^{app}_{HC,01} >> k_{Cd,01}$, if this case is operative the reactivity of the cysteine residue must be increased, presumably because the pK_a value is lowered by the neighboring histidine, thereby increasing the fraction of the cysteine side-chain that is in the reactive thiolate form.

In a second limiting case, association is primarily to form 2, i.e. $k_{1C}k_{H1} << k_{1H}k_{H2}$, and $k^{app}_{HC,01} \sim k_{H2}(k_{1H}/k_{H1})$. Because $k_{1H}/k_{H1} \sim 88$ M^{-1} (data in Fig. S3), $k_{H2} \sim 1.5 \times 10^4$ s^{-1} for this pathway to be operative with the observed rate constant ($k^{app}_{HC,01} = (1.3 \pm 0.3) \times 10^6$ $M^{-1}s^{-1}$ (Table 1)). Because $k_{Cd,01} = (5.9 \pm 0.6) \times 10^4 M^{-1}s^{-1}$, the effective concentration of Cd^{2+} in structure H is ~0.25 M.

The lowering of the pK_a of Cys and the preassociation of Cd^{2+} with His, cannot be distinguished with the current data. Of course, association cannot be

through say 2 and dissociation through C without recourse to "perpetual motion".

5. Binding of Cd^{2+} ion to the histidine residue of P_H

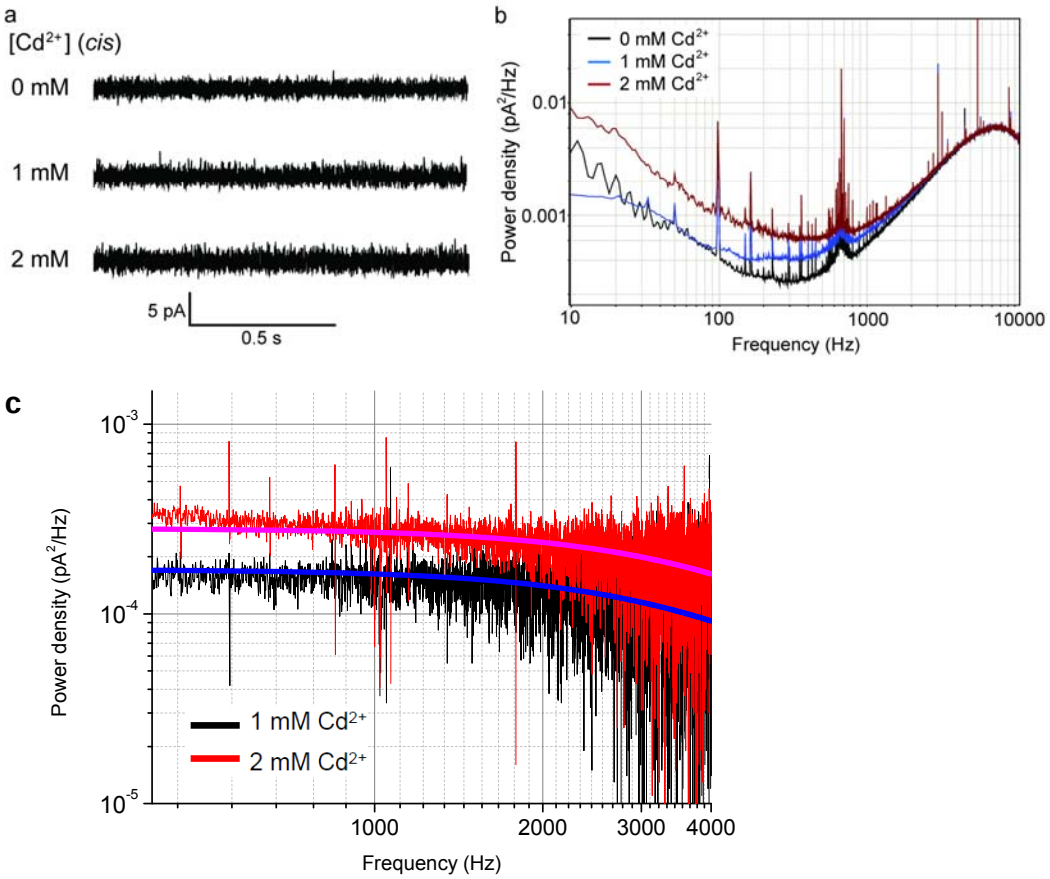

Figure S3. Reversible binding of Cd^{2+} ion to P_H. (*A*) Stacked current recording traces of $(AG)_6(L135H\text{-}AG)_1$), P_H, at different concentrations of $Cd(NO_3)_2$ (*cis*). Experimental conditions were the same as in Fig. 5 of the main text. The traces were acquired with a low-pass 4-pole Bessel filter set at 10 kHz and acquired at 100 kHz. The excerpts shown are digitally low-pass filtered at 1000 Hz. The transient binding of Cd^{2+} does not produce a new discrete current level, instead it increases the signal noise. (*B*) Current power spectra of the three traces shown in (*A*). (*C*) Current power spectra at 1 and 2 mM Cd^{2+} after the subtraction of the background (no Cd^{2+}). The spectra are fitted to Lorentzian distributions, with the current blockade by Cd^{2+} taken to be 4 pA, to obtain the association and dissociation rate constants of Cd^{2+}, and hence the equilibrium dissociation constant (7,8): $k_{H,01}$ = (2.2 ± 0.1) × 10^6 $M^{-1}s^{-1}$; $k_{H,10}$ = (2.5 ± 0.4) × 10^4 s^{-1}; $K_{d,H}$ = (1.1 ± 0.2) × 10^{-2} M (n = 2).

SUPPORTING REFERENCES

1. Greenwood, N. N., and A. Earnshaw. 1984. Chemistry of the Elements; Permagon Press/New York. 1185–1187.
2. Nan, J., and X.-P. Yan. 2010. A circular dichroism probe for L-cysteine based on the self-assembly of chiral complex nanoparticles. Chem. Eur. J. 16:423–427.
3. Shen, J.-S., D.-H. Li, M.-B. Zhang, J. Zhou, H. Zhang, and Y.-B. Jiang. 2011. Metal−metal-interaction-facilitated coordination polymer as a sensing ensemble. Langmuir 27:481–486.
4. Shen, J.-S., D.-H. Li, Q.-G. Cai, and Y.-B. Jiang. 2009. Highly selective iodide-responsive gel-sol state transition in supramolecular hydrogels. J. Mater. Chem. 19:6219–6214.
5. Andersson, L.-O. 1972. Study of some silver-thiol complexes and polymers: stoichiometry and optical effects. J. Polym. Sci., Part A-1 10:1963–1973.
6. Colquhoun, D., and A. G. Hawkes. 2009. The principles of the stochastic interpretation of ion-channel mechanisms. In Single-channel recording. B. Sakmann, and E. Neher, editors. Springer/New York, London. 397–482.
7. DeFelice, L. J. 1981. Introduction to Membrane Noise. Plenum Press/New York. 296–313.
8. Verveen, A. A., and L. J. DeFelice. 1974. Membrane noise. Prog. Biophys. Mol. Biol. 28:189–265.